Focal-plane Wavefront Sensing for Active Optics in the VST Based on an Analytical Optical Aberration Model

R. Holzlöhner[a], S. Taubenberger[a], A. P. Rakich[b,a], L. Noethe[a], P. Schipani[c] and K. Kuijken[d]

[a]European Southern Observatory (ESO), Karl-Schwarzschild-Str. 2, D-85748 Garching, Germany; [b]GMTO Corp., Pasadena, CA 91107, USA; [c]INAF - Osservatorio Astronomico di Capodimonte, Salita Moiariello 16, I-80131 Naples, Italy; [d]Leiden Observatory, Niels Bohrweg 2, NL-2333 CA Leiden, Netherlands

ABSTRACT

We study a novel focal plane wavefront sensing and active optics control scheme at the VST on Cerro Paranal, an $f/5.5$ survey telescope with a 1×1 degree field of view and a 2.6 m primary mirror. This scheme analyzes the elongation pattern of stellar PSFs across the full science image (256 Mpixels) and compares their second moments with an analytical model based on 5th-order geometrical optics. We consider 11 scalar degrees of freedom in mirror misalignments and deformations (M2 piston, tip/tilt and lateral displacement, detector tip/tilt, plus M1 figure astigmatism and trefoil). Using a numerical optimization method, we extract up to 4000 stars and complete the fitting process in under one minute. We demonstrate successful closed-loop active optics control based on maximum likelihood filtering.

Keywords: active optics, wide-field telescopes, point spread function, elongation, aberration, optical plate diagram

1. INTRODUCTION

Active optics is essential in modern large telescopes to compensate mirror misalignments and misfigure, mostly caused by temperature and gravity vector variations.[1,2] Closed-loop active optics control of wide-field telescopes is demanding both because of the tight alignment tolerances in fast optics, and also because the field dependence of aberrations in misaligned wide-field systems places tighter constraints on various system degrees of freedom than is the case with more conventional narrow field-of-view telescopes.

On the other hand, wide-field telescopes are often employed to run surveys, some of which require good PSF uniformity across the field and high overall image quality, in particular dark matter surveys such as KiDS.[3,4] Wide-field telescopes often rely on curvature wavefront sensing (CWFS) to feed their active optics systems, which analyzes highly defocused star images("donuts"), typically on the edge of the science field. However, since CWFS senses irradiance variations in the pupil induced by the second derivatives of the wavefront, the measurement errors in the low-order aberrations are higher than in Shack-Hartmann or pyramid wavefront sensors under identical conditions.[5] Moreover, CWFS can only sample a few points in the field and thus it may be advantageous to validate (and improve upon) their performance using a complimentary wavefront sensing scheme.

In this article, we continue a study of the ellipticity method, a focal plane wavefront sensing scheme without the need for additional sensor hardware.[6,7] This method solely uses science images (in the case of the VST, provided by the 256-Mpix visible light camera OmegaCAM[8]), extracts up to 4000 stars uniformly covering the entire field, and analyzes the second moments of their PSFs. The resulting pattern of PSF sizes and ellipticities is then compared with the pattern from an analytical model, based on 5th-order geometrical optics. This model expresses the star PSF second moments for the misaligned telescope with shape distortions in the primary mirror. The Levenberg-Marquardt multidimensional minimization method[9] is then applied to rapidly approximate the observation.

Further author information: (Send correspondence to R.H. E-mail: rholzloe at eso.org, Tel. +49 89 3200 6671, www.eso.org)

Table 1. Setup and environmental conditions of runs obtained during two technical nights, where the active optics of the VST was controlled with the ellipticity method in closed loop.

ID	Target	Frames	Altitude [deg]	T [°C]	DIMM [arcsec]
1	LMC	20	43.3 – 46.5	13.8 – 14.0	0.71 – 0.98
2	M41	23	56.0 – 69.2	13.5 – 14.0	0.68 – 0.93
3	Galactic bulge	32	57.2 – 40.0	14.1 – 14.3	0.66 – 0.99
4	SMC	25	38.8 – 40.8	14.3 – 14.7	0.46 – 0.94
5	LMC	48	35.4 – 42.7	11.2 – 13.7	0.71 – 2.33
6	M41	40	49.2 – 69.5	10.7 – 11.5	1.67 – 2.50
7	Fornax cluster	2	58.0 – 58.7	14.0	1.03 – 1.13

Even after exposure times of several tens of seconds, the star PSFs are still affected by residual atmospheric noise.[10] Moreover, there are occasional cases in which the minimization method yields two or more ambiguous solutions (local minima). It is therefore necessary to apply some low-pass filtering, such as Kalman filtering that is used in the active optics control system of the Very Large Telescope (VLT).[11] In this work, we successfully apply filtering based on maximum likelihood estimation.[12]

2. FIRST LIGHT FOR THE ELLIPTICITY METHOD ON THE VST

We had the opportunity to test the ellipticity method during the two technical nights of September 28/29 and 29/30, 2015. During these two nights, we controlled the VST from ESO headquarters in Germany using the newly implemented Garching Remote Access Facility (G-RAF).[13]

The typical proceedings during these nights consisted of a telescope preset to the selected field, an initialisation of the active optics control parameters (ONECAL), and two or three iterations of active optics corrections using the conventional curvature wavefront sensing ('donut') method; see Schipani *et al.*[14] for an overview of the VST active optics system. After this point, the donut method was switched off, and the active optics control was solely driven by the ellipticity method. To this end, the acquired 30 s OmegaCAM r-band images were analysed and optical aberrations were determined on a computer in Paranal, which also returned the low-pass filtered corrections to the Telescope Control Software. This enabled completely autonomous closed-loop operations, as sketched in Fig. 1.

The individual runs lasted up to two hours before a new telescope preset plus ONECAL were performed. They varied in the atmospheric conditions (DIMM seeing, temperature gradients), the altitude range of the observed field above the horizon, and the nature of the observed astronomical objects (with very different numbers of stars in the field). The aim was to investigate

- if very good image quality can be obtained under ideal atmospheric conditions (to test the actual wavefront-sensing method)
- if the active optics control remains stable and shows no divergence under all atmospheric conditions, including phases of very poor seeing (to test the applied low-pass filtering)
- how the procedure reacts to fields with different number / density of stars (to test whether the technique could be applied for general-purpose wavefront sensing)

Table 1 provides an overview of individual runs obtained during our two technical nights and lists relevant atmospheric and observing parameters.

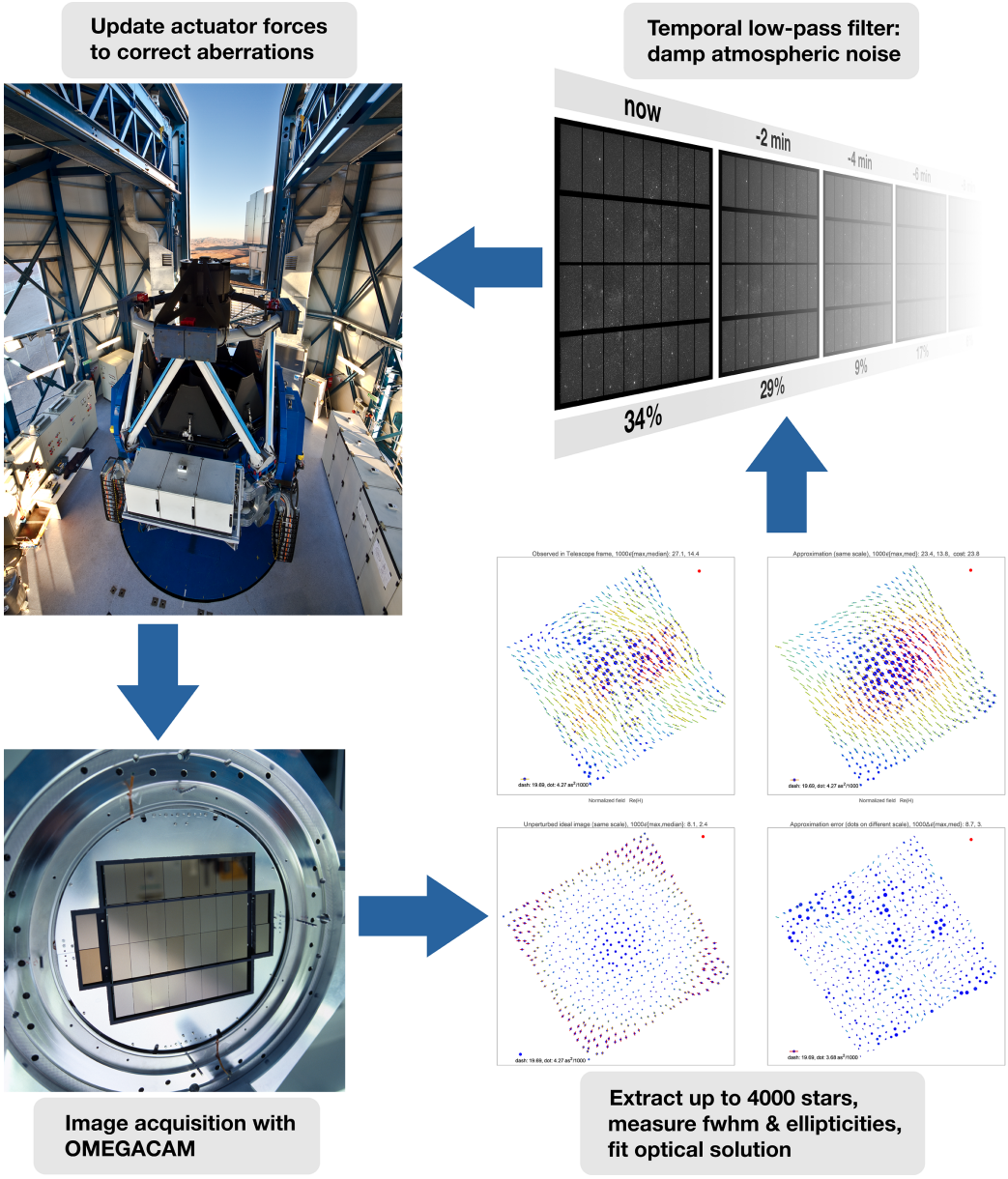

Figure 1. Closed-loop active optics control at the VST, based on focal-plane wavefront sensing. *Bottom left:* A science image is obtained with OmegaCAM (256 Mpixels, 1×1 degree field of view). *Bottom right:* Up to ∼4000 stars are automatically identified and their spot sizes and ellipticities are measured (the plot shows their medians arranged in 24×24 tiles). Optical aberrations in the field are determined by fitting an analytical aberration model to the ellipticity and spot-size pattern. This software runs in less than one minute, which is comparable to the readout time of the CCD images. *Top right:* Low-pass filtering is applied to damp atmospheric noise and calculate the most likely telescope state. Image weights fade exponentially with time and additional penalties apply for large fitting errors, large differences of the solution from previous ones and solution ambiguity. *Top left:* Actuator forces are updated to correct for the inferred optical aberrations, and the next exposure is started. Image credit: ESO, ESO/G. Lombardi

Table 2. Number of extracted stars, cost of the aberration fit, filtering time constant τ and attained image quality for the same runs described in Table 1.

ID	Extracted stars	Image quality [arcsec]	Cost	τ [min]
1	3840	0.38 – 0.63	8.8 – 88.7	3
2	$\geq$ 3834	0.35 – 0.51	5.9 – 31.2	6
3	3840	0.41 – 0.61	13.8 – 81.1	5
4	3840	0.39 – 0.56	11.9 – 44.1	5
5	3840	0.55 – 1.55	29.4 – 308.9	5
6	$\geq$ 3745	0.81 – 1.51	32.9 – 276.1	5
7	$\leq$ 944	0.40 – 0.43	10.0 – 13.8	5

3. RESULTS

As a general result one can register that our focal-plane ellipticity wavefront sensing scheme at the VST works reliably under a variety of conditions. After some initial parameter adjustments based on a set of calibration images, it has been possible to control the VST active optics flawlessly in closed loop during two full nights. In periods of good seeing, the fitted aberration solution was excellent (cost $\leq$ 20), the residual aberrations very small, and the resulting image quality superb (see Table 2). By 'cost' we mean the average squared difference between the measurements and the numerical approximation, hence the total fitting error.

The only glitches occurred when the telescope was pointed to a rather sparse field (Run #7), and the software repeatedly issued warnings that an insufficient number of stars had been extracted, although in retrospect the obtained solutions look good in terms of costs (see also Section 3.4). Apart from that, even large changes, such as a 70 μm drift in focus over two hours in Run #5, were reliably and promptly corrected with a time lag of about two frames owing to the low-pass filtering (Kalman filtering with a position/velocity approach can reduce this lag using linear prediction).

In the following, the influence of low-pass filtering time constant τ, the performance under poor seeing conditions, the correlations of aberrations with external parameters, and the application of the method to sparse fields will be illuminated in more detail.

3.1 Low-pass filtering: effective damping of atmospheric noise

By far the biggest source of uncertainty in (focal-plane) wavefront sensing is noise introduced by atmospheric turbulence. Even with exposure times of 30 s and more, which are common in photometric surveys and which we have used throughout the technical nights, atmospheric turbulence leads to residual wavefront errors similar to those from typical telescope misalignments. Effective damping of atmospheric noise through low-pass filtering is therefore essential. We have adopted a maximum likelihood estimation of the current telescope misalignment state, in which the aberrations processed from a frame with the sequence number i is weighted by the weight w_i that equals the inverse of summed penalties, consisting of the age of the frame $t_0 - t_i$, where t_0 is the current time, the altitude difference from the current altitude, the costs of the aberration parameter fit and its degeneracies, and the distance of the solution from previous ones (the latter is implemented carefully with the purpose of suppressing extreme outlier results, rather than introducing an additional driver of low-pass filtering). The weights w_i are calculated as

$$w_i = \frac{\widetilde{w}_i}{\sum_{j=0}^{\infty} \widetilde{w}_{i-j}}, \tag{1}$$

$$\frac{1}{\widetilde{w}_i} = \exp\left(-\frac{t_0 - t_i}{\tau}\right) + \sum_k p_i^{(k)} \tag{2}$$

where the additional penalties $p_i^{(k)}$ depend linearly or quadratically on the quantity to be penalized. The advantage of defining penalties and weighting the corrections gleaned from individual frames by their inverse

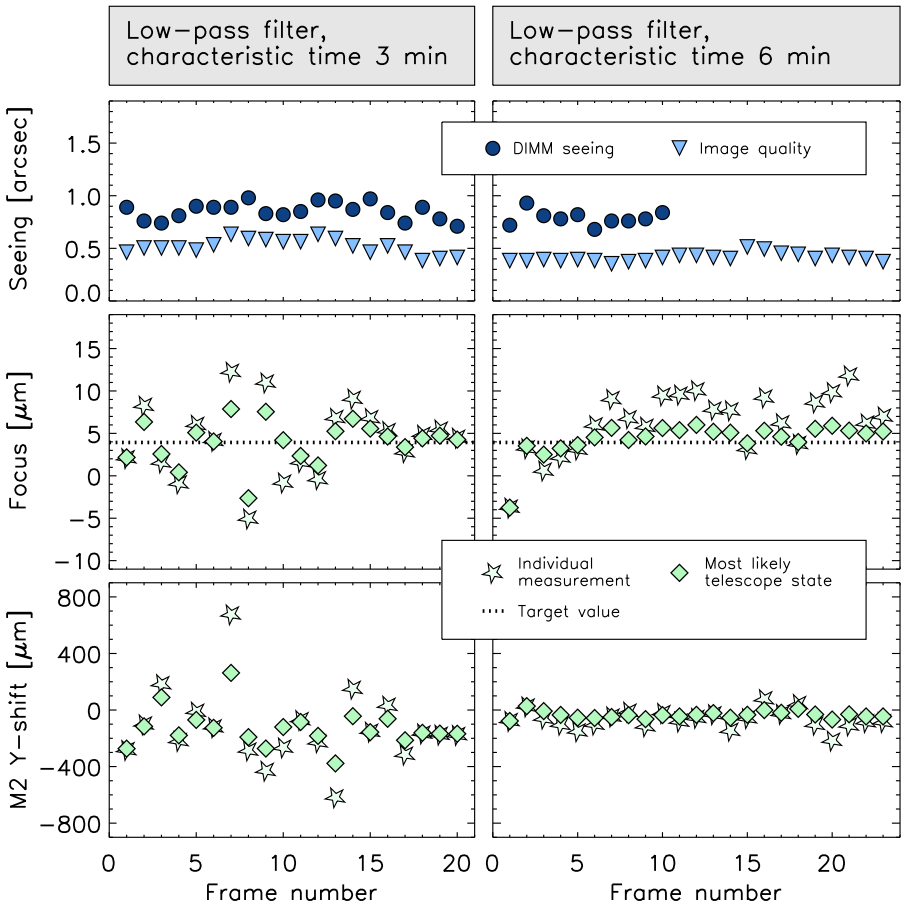

Figure 2. Effect of different time constants τ in the low-pass filtering. Two runs (#1 and #2 from Tables 1 and 2) with similar atmospheric conditions (DIMM seeing), but different τ of 3 min (left-hand panels) and 6 min (right-hand panels) are compared. Too weak filtering leads to an enhanced scatter in the inferred most likely telescope focus (green diamonds), but also in the individual single-frame focus measurements (pale green stars). The latter may be due to overshooting active optics corrections. Stronger filtering leads to smoother corrections and a more consistent and on average better image quality.

sum is that any single large penalty can render w_i small (*e.g.*, an image taken hours ago has no bearing on the current most likely telescope aberration state, not even if the quality of its fit was high and all other conditions like telescope altitude are similar).

During or test runs we experimented with different filtering parameters. In particular, the characteristic time scale τ, after which the temporal penalty of an image increases by factor e, has been varied. An initial value of $\tau = 3\,\mathrm{min}$, turned out to be too short. Given a typical cadence with 2–3 min delay between frames (30 s exposure + 45 s readout + 1 min image analysis), a 3 min e-folding time means that under most circumstances only two frames have non-negligible weight in the determination of the most likely telescope aberrations. As can be seen in the left-hand panels of Fig. 2, this resulted in insufficient damping of atmospheric noise, and a jumpy behaviour with frequent overcorrections. An increase of τ to 5–6 min, corresponding to the consideration of the last 3–4 frames in the determination of the most likely telescope state (right-hand panels of Fig. 2), solved this problem, leading to smaller fluctuations and on average better image quality without rendering the control too sluggish.

3.2 Stability under poor seeing conditions

The biggest concern in our focal-plane wavefront sensing approach was the impact of noise introduced by atmospheric turbulence. The residual contributions of turbulence to the aberrations decay only very slowly, and for exposure times of tens of seconds there is a non-negligible atmospheric contribution, especially if the seeing is poor.[10] During the two technical nights which we could use for our tests, we had periods of good as well as periods of very bad seeing (see Table 1), so that we could investigate how the method performs under these conditions.

The upshot is that our active optics control remains stable even when the DIMM seeing lies around 2.5 arcsec (Fig. 3, right-hand panels). The aberrations determined in single frames show a strongly increased scatter owing to atmospheric noise, but the low-pass filtering still works as intended: Poor-seeing images are assigned low weights, and as a result a larger number of frames are considered in the weighted average, leading to stronger low-pass filtering.

It is worth noting that the strong filtering does *not* lead to a loss of corrective power: Systematic trends over longer time scales are still recognised and corrected, as can be seen in the cumulative focus corrections in the bottom-right panel in Fig. 3.

Our telescope aberration model includes three scalar modes that cannot be corrected: These are spherical aberration (SA) and detector tip/tilt. SA is nearly degenerate with defocus in the ellipticity method as mentioned in Subsection 2.4 of reference[7] (more precisely, a singular value decomposition analysis of the fitting cost vs. defocus and SA reveals the existence of two related eigenmodes, one equal to the sum of defocus and SA and the other to their difference, the latter with a singular value of vanishing magnitude). However, we do include a fixed value of 20 nm RMS in spherical aberration in the model, which causes the target value of optimal defocus to shift from zero to 3.9 μm.

The situation with the detector tip/tilt is somewhat different: In contrast to SA, we can actually quantify this misalignment with acceptable accuracy along with the 9 other misalignments. However, detector tip/tilt cannot be corrected in OmegaCAM except through a cumbersome shimming procedure. Similar to SA vs. defocus, we validated that detector tip/tilt of up to one arcminute can be approximately compensated by an M2 rotation about a point located 1667.64 mm behind the M2 vertex (the coma neutral rotation point, for comparison, lies 1165 mm behind M2). Again, this shifts the target value of M2 lateral vertex position and rotation to nonzero values.

3.3 Correlations of aberrations with external parameters

External parameters are known to have an impact on telescope aberrations. Most notably these are the telescope pointing (in the case of an alt-azimuth telescope such as the VST only the altitude), owing to the variation of the gravity vector, and the temperature causing thermal expansion of the telescope structure. These effects can be modeled easily, and at least the temperature drift of the focus is in many (also passive) telescopes to first order corrected in open loop using lookup tables.

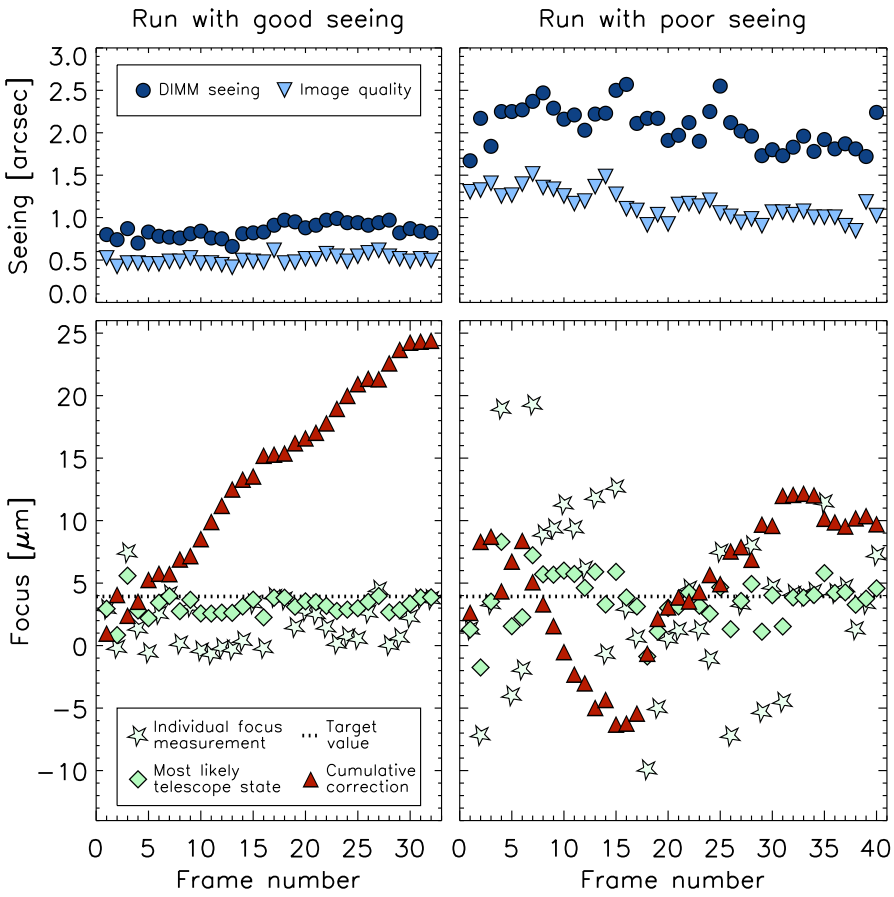

Figure 3. Reliability of focal-plane wavefront sensing under poor seeing conditions. The figure compares a good-seeing (left-hand panels) with a bad-seeing (right-hand panels) run (#3 and #6 from Tables 1 and 2). Closed-loop active optics corrections were enabled and hence the most likely telescope focus after low-pass filtering of the individual measurements (green diamonds) never deviates strongly from the target value of 3.9 μm, even though the individual single-frame measurements of telescope focus (pale green stars) show a much larger scatter if additional noise is introduced by strong atmospheric turbulence. The cumulative focus corrections (red triangles), however, reveal that without significant active optics adjustments strong focus drifts would have been observed.

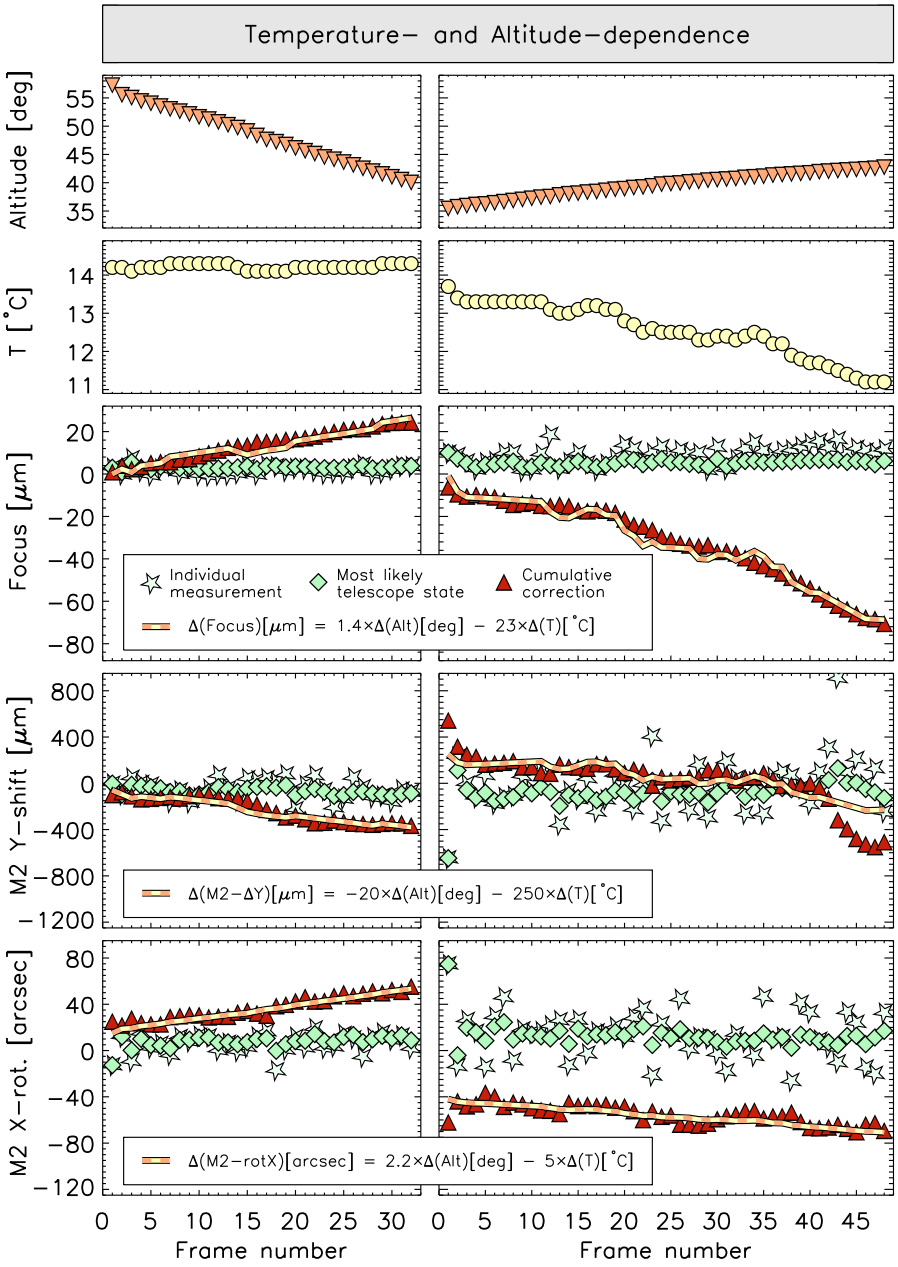

Figure 4. Temperature- and altitude-dependence of optical aberrations as determined with focal-plane ellipticity wavefront sensing. Two runs are shown: one with strong altitude variation and almost constant temperature (left-hand panels, #3 from Tables 1 and 2), and one with comparatively moderate altitude changes but a strong temperature gradient (right-hand panels, #5 from Tables 1 and 2). From top to bottom, the panels depict the temporal behaviour of altitude, temperature, focus, M2 lateral displacement in Y-direction, and M2 rotation around the X-axis (the latter two are along the gravity vector). Closed-loop active optics corrections were enabled, and hence the individual single-frame measurements of the aberrations (pale green stars) as well as the most-likely telescope state after low-pass filtering of the individual measurements (green diamonds) never deviate strongly from the target value. The cumulative corrections (red triangles), however, show that this is only by virtue of massive cumulative active optics adjustments. The temperature and altitude fit of the selected aberrations is overlayed and compared with the cumulative corrections.

During our test nights at the VST, however, no open-loop corrections were applied, and the full adjustment was left to our closed-loop active optics control program. Therefore, the applied cumulative corrections contain the full temperature and altitude dependence. We used our data to fit these dependencies (see Fig. 4), and compared the fit coefficients with those measured in previous data where the wavefront-sensing was accomplished using the CWFS (donut method). The coefficients for the temperature and altitude dependence of focus, as well as the altitude dependence of M2 rotation and lateral displacement, all agreed within 25% between the two different methods. Given the statistical limitations (we had only one run with significant temperature gradient), this level of agreement is good and tells us that focal-plane ellipticity wavefront sensing is capable of capturing telescope aberrations correctly.

Specifically, we obtained the following temperature and altitude dependencies:

$$\Delta(\mathrm{FOCUS})\,[\mu\mathrm{m}] = 1.4\ (1.4) \times \Delta(\mathrm{ALT})\,[\mathrm{deg}] - 23\ (-27) \times \Delta T\,[K] \tag{3}$$

$$\Delta(\mathrm{M2\text{-}Y})\,[\mu\mathrm{m}] = -20\ (25) \times \Delta(\mathrm{ALT})\,[\mathrm{deg}] - 250\ (-0.5) \times \Delta T\,[K] \tag{4}$$

$$\Delta(\mathrm{M2\text{-}rotX})\,[\mathrm{arcsec}] = 2.2\ (2.7) \times \Delta(\mathrm{ALT})\,[\mathrm{deg}] - 5\ (0) \times \Delta T\,[K], \tag{5}$$

where the numbers in parentheses are obtained from fits of several months of telemetry data (some are currently implemented in lookup tables).

The temperature coefficient for focus of $23\,\mu\mathrm{m\,K^{-1}}$ is roughly compatible with the coefficient of thermal expansion of steel of $12 \times 10^{-6}\,\mathrm{K^{-1}}$: $23\,\mu\mathrm{m\,K^{-1}} / 12 \times 10^{-6}\,\mathrm{K^{-1}} \approx 1.9\,\mathrm{m}$, which is about 50% less than the physical distance M1–M2. The difference might have to do with the fact that we did not monitor the actual telescope temperature, but used the ambient outside temperature for the correlations that is logged in the FITS image file headers.

In conclusion one can state that known dependencies of telescope aberrations on external parameters are reproduced by our focal-plane wavefront sensing approach at the VST. These known drifts are predictable and should be corrected in open loop. In this way, the otherwise inevitable time lag from using a non-predictive low-pass filter in the closed-loop active optics corrections can be avoided.

3.4 Observations of sparse fields

In focal-plane wavefront sensing the information contained in a single stellar PSF is very limited. For the ellipticity method to work and deliver accurate and reliable results, it is necessary to sample hundreds to thousands of stellar PSFs, as evenly distributed as possible across the field of view. For this reason, during most of the two technical nights the VST was pointed to fields particularly rich of stars, such as the Galactic Bulge, the Magellanic Clouds, or along the Orion Arm. In these fields, the software always extracted a number of stars very close to the hardcoded maximum of 3840 (see Table 2). However, under real-life conditions, the fields observed by a survey telescope are not always that rich in stars. Quite the contrary is true for surveys such as VST ATLAS and KiDS,[4, 15] which target extragalactic objects and explicitly avoid the Galactic Plane (Fig. 5).

An important test therefore consisted in evaluating the performance of focal-plane wavefront sensing in sparse fields. We pointed the VST to the Fornax galaxy cluster at a high Galactic latitude of -57 degrees (Run #7 in Tables 1 and 2). In this field, the software extracted fewer than 1000 stars that matched the signal-to-noise criteria. Worried by regular warnings issued by the software, we terminated the experiment after only three images had been obtained. However, in retrospect it appears that the software was still able to find decent solutions for the optical aberrations with low costs (see Table 2). Further testing is definitely needed to investigate how stable and reliable the wavefront sensing with relatively few stars in the field can be, and hence whether the ellipticity method can be used as an all-purpose wavefront-sensing technique in wide-field telescopes. Such a study should be of particular interest to the Large Synoptic Survey Telescope (LSST) which will have a clear aperture of 8.36 m and a field of view of 3.5 degrees and is aiming to achieve outstanding image quality and PSF uniformity.

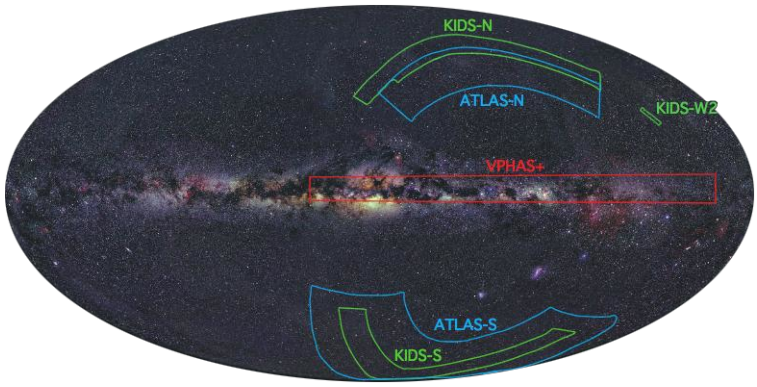

Figure 5. Survey areas of the VST ATLAS, KiDS and VPHAS+ surveys. Credit: ESO.

4. CONCLUSIONS

We have complemented our focal-plane ellipticity wavefront sensing method,[7] based on 5th-order geometrical optics, by an active optics control method. We apply maximum likelihood estimation (MLE) to find the most likely telescope misalignment and misfigure state and correct the alignment in closed loop. During two technical nights in September 2015, we have successfully driven the VST wide-field survey telescope using our algorithm, implemented in *Mathematica* and running directly on the instrument workstation in Paranal. The scheme does not require additional wavefront sensing hardware and can run in parallel to a survey cadence. We argue that since the method operates directly on the scientifically relevant PSF shape across the full field, it can yield superior correction fidelity compared to other schemes like curvature wavefront sensing.

It remains to be determined if the 5th-order geometrical optics model (which essentially links a Taylor expansion of the wavefront error to certain mirror misalignments and shape distortions) is accurate enough for other wide-field telescopes such as VISTA or the LSST. Any closed-loop active optics control scheme ought to be complemented by an accurately calibrated open-loop model (*i.e.*, lookup tables to correct for variable temperature and telescope altitude angle). The MLE filter could be extended to full Kalman filtering with linearly predictive capabilities.

REFERENCES

[1] Noethe, L., "Use of minimum energy modes for modal-active optics corrections of thin meniscus mirrors," *J. Mod. Opt.* **38**, 1043–1066 (1991).

[2] Noethe, L., "Active Optics in Modern, Large Optical Telescopes," in [*Progress in Optics*], Wolf, E., ed., **43**, 3–69, Elsevier (2002).

[3] Kuijken, K., "Lensing with KiDS," in [*KITP Program: Applications of Gravitational Lensing: Unique Insights into Galaxy Formation and Evolution*], (Oct. 2006).

[4] Kuijken, K., Heymans, C., and Hildebrandt, H., *et al..*, "Gravitational lensing analysis of the Kilo-Degree Survey," *Monthly Notices Royal Astron. Soc.* **454**, 3500–3532 (Dec. 2015).

[5] Fienup, J. R., Thelen, B. J., Paxman, R. G., and Carrara, D. A., "Comparison of Phase Diversity and Curvature Wavefront Sensing," *Proc. SPIE* **3353**, 930 (1998).

[6] Noethe, L., Schipani, P., Holzlöhner, R., and Rakich, A., "A method for the use of ellipticities and spot diameters for the measurement of aberrations in wide-field telescopes," *Adv. Opt. Tech.* **3**, 315–333 (Jun 2014).

[7] Holzlöhner, R., Rakich, A., Noethe, L., Kuijken, K., and Schipani, P., "Fast active optics control of wide-field telescopes based on science image analysis," *Proc. SPIE* **9151**, 87 (Jun 2014).

[8] Kuijken, K., Bender, R., and Cappellaro, E., *et al.*, "OmegaCAM: wide-field imaging with fine spatial resolution," in [*Ground-based Instrumentation for Astronomy*], Moorwood, A. F. M. and Iye, M., eds., *Proc. SPIE* **5492**, 484–493 (Sept. 2004).

[9] Levenberg, K., "A method for the solution of certain non-linear problems in least squares," *Quarterly of Appl. Math.* **2**, 164–168 (1944).

[10] Roddier, F., Roddier, D., Northcott, M. J., Graves, J. E., and McKenna, D. L., "One-dimensional spectra of turbulence-induced Zernike aberrations: time-delay and isoplanicity error in partial adaptive compensation," *"J. Opt. Soc. Am. A"* **10**, 957–965 (May 1993).

[11] Guisard, S., Noethe, L., Spyromilio, J., and Delgado, F., "Performance and improvement of active optics at the very large telescope," *Proc. SPIE* **4837**, 637–648 (2003).

[12] Pfanzagl, J. and Hamböker, R., [*Parametric statistical theory*], Walter de Gruyter, Berlin (1994). ISBN 3-11-013863-8.

[13] Kjeldsen, H., "Draft minutes 39th meeting," tech. rep., ESO Users' Committee (April 2015).

[14] Schipani, P., Noethe, L., and Magrin, D., *et al..*, "The Active Optics system of the VLT Survey Telescope," *"Appl. Opt."* **55**, 1573–1583 (2016).

[15] Shanks, T., Metcalfe, N., and Chehade, B., *et al..*, "The VLT Survey Telescope ATLAS," *"Monthly Notices Royal Astron. Soc."* **451**, 4238–4252 (Aug. 2015).